Supplementary Material (ESI) for Chemical Science

Supporting information for

Conservation of structural arrangements and 3:1 stoichiometry in a series of crystalline conductors of TMTTF, TMTSF, BEDT-TTF, and chiral DM-EDT-TTF with the oxo-bis[pentafluorotantalate(V)] dianion

Nabil Mroweh,[a] Cécile Mézière,[a] Magali Allain,[a] Pascale Auban-Senzier,[b] Enric Canadell*[c] and Narcis Avarvari*[a]

[a] MOLTECH-Anjou, UMR 6200, CNRS, UNIV Angers, 2 bd Lavoisier, 49045 ANGERS Cedex, France. E-mail: narcis.avarvari@univ-angers.fr

[b] Laboratoire de Physique des Solides, Université Paris-Saclay, CNRS UMR 8502, 91405 Orsay, France

[c] Institut de Ciència de Materials de Barcelona (CSIC), Campus de la UAB, E-08193 Bellaterra, Spain. E-mail: canadell@icmab.es

Experimental section

General comments. Nuclear magnetic resonance spectra were recorded on a Bruker Avance DRX 300 spectrometer operating at 282 MHz for 19F. Chemical shifts are expressed in parts per million (ppm). The following abbreviations are used: s, singlet; d, doublet; m, multiplet. A Bruker Esquire 3000 plus spectrometer was used for electrospray ionization mass spectrometry (ESI-MS). Elemental analysis were recorded using Flash 2000 Fisher Scientific Thermo Electron analyzer.

Synthesis of (n-Bu$_4$N)$_2$TaF$_{10}$O and (n-Bu$_4$N)TaF$_6$

Method 1. The procedure used for the synthesis of (n-Bu$_4$N)PF$_6$ (J. M. Braam, C. D. Carlson, D. A. Stephens, A. E. Rehan, S. J. Compton and J. M. Williams, *Inorg. Synth.*, 1986, **24**, 130–143) has been adapted to the preparation of (n-Bu$_4$N)TaF$_6$, according to the transformations:

TaF$_5$ + HF $\rightarrow$ HTaF$_6$ / HTaF$_6$ + (n-Bu$_4$N)HSO$_4$ $\rightarrow$ (n-Bu$_4$N)TaF$_6$
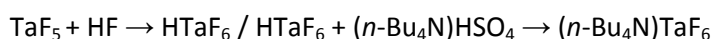
The experiment was carried out in plastic equipment. HF (48% in water, 7.2 mL, d = 1.15, 4 g, 0.20 mol) was added slowly to TaF$_5$ (5 g, 0.018 mol). After twenty minutes of stirring, the yellow solution of HTaF$_6$ thus obtained was added to a solution of (n-Bu$_4$N)HSO$_4$ (6.8 g, 0.020 mol) dissolved in the minimum of water. The white precipitate which immediately appeared was recovered by filtration and washed with water until neutral. The solid was purified by dissolution in dichloromethane, drying with MgSO$_4$ and precipitation with diethyl ether. However, according to the ^{19}F NMR spectra the solid thus obtained is a mixture of (n-Bu$_4$N)TaF$_6$ and (n-Bu$_4$N)$_2$Ta$_2$F$_{10}$O (Fig. S1). Upon conservation in aerobic conditions the mixture slowly evolves towards exclusive presence of (n-Bu$_4$N)$_2$Ta$_2$F$_{10}$O.

Methanolic hydrolysis of (n-Bu$_4$N)TaF$_6$ in the presence of (n-Bu$_4$N)OH, according to ref. 41 (J. Sala-Pala, J. Y. Calves, J. E. Guerchais, S. Brownstein, J. C. Dewan and A. J. Edwards, *Can. J. Chem.*, 1978, **56**, 1545–1548) provides (n-Bu$_4$N)$_2$Ta$_2$F$_{10}$O in quantitative manner.

2 (n-Bu$_4$N)TaF$_6$ + (n-Bu$_4$N)OH $\rightarrow$ (n-Bu$_4$N)$_2$Ta$_2$F$_{10}$O + (n-Bu$_4$N)F + HF
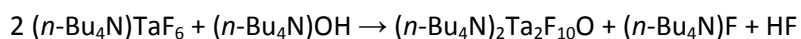
Recrystallization from a 50/50 mixture of dichloromethane and ethyl acetate gives small translucent crystalline blocks. The crystalline solid, which is analytically pure (n-Bu$_4$N)$_2$Ta$_2$F$_{10}$O, was used in electrocrystallization with TMTTF, TMTSF, BEDT-TTF and DM-EDT-TTF.

m.p. 202-204°C. ^{19}F NMR (CD$_2$Cl$_2$): 9 (m, 2F$_{ax}$), 32 (d, 8F$_{eq}$) (Fig. S1). MS (ESI, m/z): 810 [M − (n-Bu$_4$N)]$^-$. Elemental analysis calcd (%) for C$_{32}$H$_{72}$F$_{10}$N$_2$OTa$_2$: C 36.51, H 6.89, N 2.66; found: C 36.20, H 6.77, N 2.70.

Method 2. The procedure described by Brownstein was followed (S. Brownstein, *Inorg. Chem.*, 1973, **12**, 584–589):

(n-Bu$_4$N)BF$_4$ + TaF$_5$ → (n-Bu$_4$N)TaF$_6$ (+ BF$_3$)
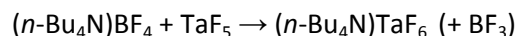
TaF$_5$ (1 g, 3.62 mmol, kept in a glove box) and (n-Bu$_4$N)BF$_4$ (1.19 g, 3.62 mmol) are respectively placed in 25 mL of degassed dichloromethane (HPLC grade). The latter was added slowly to the former under stirring. After one hour the solvent and the boron trifluoride formed are evaporated using the rotavapor. The solid thus obtained is recrystallized from a 50/50 mixture of dichloromethane and ethyl acetate to give 1.42 g of a white microcrystalline powder (yield 73%). According to the ^{19}F NMR spectra the solid contains only (n-Bu$_4$N)TaF$_6$ with no trace of (n-Bu$_4$N)$_2$Ta$_2$F$_{10}$O (Fig. S2).

m.p. 218-220°C. ^{19}F NMR (CD$_2$Cl$_2$): 39 (s, broad). MS (ESI, m/z): 295 (M$^+$). Elemental analysis calcd (%) for C$_{16}$H$_{36}$F$_6$NTa: C 35.76, H 6.75, N 2.61; found: C, 35.92; H, 6.78; N, 2.56.

Method 3. A variation of Method 2 has been equally tested according to the transformation:

KTaF$_6$ + (n-Bu$_4$N)Br → (n-Bu$_4$N)TaF$_6$ + KBr
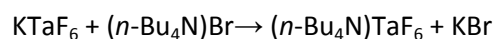
KTaF$_6$ (0.5 g, 1.50 mmol, kept in a glove box) and (n-Bu$_4$N)Br (0.48 g, 1.50 mmol) were respectively placed in 25 mL of degassed dichloromethane (HPLC grade). The latter one was added slowly to the former under stirring. After one hour, the KBr formed was removed by filtration (fritted glass funnel N° 4). Then the solvent was evaporated using the rotavapor and the resulting solid recrystallized from a 50/50 mixture of dichloromethane and ethyl acetate to give 0.62 g of a white microcrystalline powder (yield 77%).

Elemental analysis calcd (%) for C$_{16}$H$_{36}$F$_6$NTa: C 35.76, H 6.75, N 2.61; found: C 35.97, H 6.78, N 2.68.

X-Ray structure determinations

Details about data collection and solution refinement are given in Table S1 (ESI). Data collections were performed on a BRUKER KappaCCD diffractometer, equipped with a graphite monochromator utilizing MoKα radiation (λ = 0.71073Å) for $(n\text{-Bu}_4\text{N})_2\text{Ta}_2\text{F}_{10}\text{O}$, $(\text{TMTTF})_3\text{Ta}_2\text{F}_{10}\text{O}$, $(\text{TMTSF})_3\text{Ta}_2\text{F}_{10}\text{O}$ and $(\text{BEDT-TTF})_3\text{Ta}_2\text{F}_{10}\text{O}$ and on a Rigaku Oxford Diffraction SuperNova diffractometer equipped with an Atlas CCD detector and micro-focus Cu-K_α radiation (λ = 1.54184 Å) for $[(rac)\text{-DM-EDT-TTF}]_3\text{Ta}_2\text{F}_{10}\text{O}$, $[(S,S)\text{-DM-EDT-TTF}]_3\text{Ta}_2\text{F}_{10}\text{O}$ and $(n\text{-Bu}_4\text{N})\text{TaF}_6$. The structures were solved by direct methods and refined on F^2 by full matrix least-squares techniques with SHELX programs[1] (SHELXS 97 or 2013 and SHELXL 97 or 2016) using the WinGX graphical user interface.[2] All non-H atoms were refined anisotropically and absorption was corrected by Gaussian technique for $(\text{TMTSF})_3\text{Ta}_2\text{F}_{10}\text{O}$ or multiscan empirical absorption was corrected using SADABS program[3] (Sheldrick, Bruker, 2008) for $(n\text{-Bu}_4\text{N})_2\text{Ta}_2\text{F}_{10}\text{O}$, $(\text{TMTTF})_3\text{Ta}_2\text{F}_{10}\text{O}$ and $(\text{BEDT-TTF})_3\text{Ta}_2\text{F}_{10}\text{O}$ and CrysAlisPro program[4] for $[(rac)\text{-DM-EDT-TTF}]_3\text{Ta}_2\text{F}_{10}\text{O}$, $[(S,S)\text{-DM-EDT-TTF}]_3\text{Ta}_2\text{F}_{10}\text{O}$ and $(n\text{-Bu}_4\text{N})\text{TaF}_6$. The H atoms were placed at calculated positions and refined using a riding model. For $(\text{BEDT-TTF})_3\text{Ta}_2\text{F}_{10}\text{O}$ and $[(rac)\text{-DM-EDT-TTF}]_3\text{Ta}_2\text{F}_{10}\text{O}$ a statistical disorder was applied to lead to various occupation rates: for compound $(\text{BEDT-TTF})_3\text{Ta}_2\text{F}_{10}\text{O}$ one ethylene part with 0.68/0.32 occupancy factors and for $[(rac)\text{-DM-EDT-TTF}]_3\text{Ta}_2\text{F}_{10}\text{O}$ three ethylene parts with almost 0.5 occupancy factor each. The compound $(n\text{-Bu}_4\text{N})\text{TaF}_6$ has been treated as a twinned structure. Crystallographic data for the six structures have been deposited with the Cambridge Crystallographic Data Centre, deposition numbers CCDC 1999620 for $(n\text{-Bu}_4\text{N})_2\text{Ta}_2\text{F}_{10}\text{O}$, 1999621 for $(\text{TMTTF})_3\text{Ta}_2\text{F}_{10}\text{O}$, 1999622 for $(\text{TMTSF})_3\text{Ta}_2\text{F}_{10}\text{O}$, 1999623 for $(\text{BEDT-TTF})_3\text{Ta}_2\text{F}_{10}\text{O}$, 1999625 for $[(rac)\text{-DM-EDT-TTF}]_3\text{Ta}_2\text{F}_{10}\text{O}$, 1999626 for $[(S,S)\text{-DM-EDT-TTF}]_3\text{Ta}_2\text{F}_{10}\text{O}$, 2003148 for $(n\text{-Bu}_4\text{N})\text{TaF}_6$. These data can be obtained free of charge from CCDC, 12 Union road, Cambridge CB2 1EZ, UK (e-mail: deposit@ccdc.cam.ac.uk or http://www.ccdc.cam.ac.uk).

[1] G. M. Sheldrick, *Acta Crystallogr., Sect. A: Found. Crystallogr.*, 2008, **64**, 112–122.

[2] L. J. Farrugia, *J. Appl. Cryst.*, 2012, **45**, 849–854.

[3] SADABS-V2008/1 (**2008**) - Bruker AXS area detector scaling and absorption correction.

[4] CrysAlisPro 1.171.38.46 (Rigaku Oxford Diffraction, **2015**) - Empirical absorption correction using spherical harmonics, implemented in SCALE3 ABSPACK scaling algorithm.

Table S1a Crystal Data and Structure Refinement for **(n-Bu₄N)₂Ta₂F₁₀O, (TMTTF)₃Ta₂F₁₀O, (TMTSF)₃Ta₂F₁₀O**

| Compound	$(n\text{-Bu}_4N)_2Ta_2F_{10}O$	$(TMTTF)_3Ta_2F_{10}O$	$(TMTSF)_3Ta_2F_{10}O$
Empirical formula	$C_{32}H_{72}F_{10}N_2OTa_2$	$C_{30}H_{36}F_{10}OS_{12}Ta_2$	$C_{30}H_{36}F_{10}OSe_{12}Ta_2$
Molecular weight	1052.81	1349.29	1912.01
T (K)	293(2)	293(2)	293(2)
Wavelength (Å)	0.71073	0.71073	0.71073
Crystal system	Monoclinic	Triclinic	Triclinic
Space group	$C2/c$	P-1	P-1
a (Å)	21.230(2)	7.8130(1)	7.8356(9)
b (Å)	14.206(1)	10.960(1)	10.993(1)
c (Å)	18.083(2)	13.091(1)	13.558(2)
α(deg)	90	86.153(7)	90.28(1)
β(deg)	124.97(4)	78.048(4)	80.09(1)
γ(deg)	90	77.49(1)	77.836(8)
V (Å³)	4469.1(7)	1070.4(2)	1123.6(2)
Z	4	1	1
D_c (g cm⁻³)	1.565	2.093	2.826
F(000)	2088	652	868
Abs coeff (mm⁻¹)	4.959	5.764	14.653
Crystal size (mm³)	0.307× 0.246 × 0.198	0.317 × 0.215 × 0.130	0.177 × 0.173 × 0.169
θ (min / max)	3.279 / 30.035	3.634 / 27.490	3.706 / 27.722
Transmission (min/max)	0.271 / 0.375	0.289 / 0.473	0.053 / 0.084
Data collected/unique	36887 / 6425	17008 / 4857	21600 / 5179
Data observed	3880	4146	3988
R (int)	0.0589	0.0424	0.0449
Flack parameter	-	-	-
GOF on F^2	1.152	1.078	1.087
Final R indices[a] [$I > 2\sigma(I)$]	$R_1 = 0.0439$, w$R_2 = 0.0760$	$R_1 = 0.0367$, w$R_2 = 0.1062$	R1 = 0.0287, wR2 = 0.0544
R indices (all data)	$R_1 = 0.0966$, w$R_2 = 0.0963$	$R_1 = 0.0561$, w$R_2 = 0.1277$	R1 = 0.0520, wR2 = 0.0617
Largest peak in final: difference (e A⁻³)	1.662 / -1.072	1.451 / -1.868	0.687 / -1.300

[a] $R(F) = \Sigma||F_o| - |F_c||/\Sigma|F_o|$; $wR\ (F^2) = [\Sigma[w(F_o^2 - F_c^2)^2]/\Sigma[w(F_o^2)^2]]^{1/2}$

Table S1b Crystal Data and Structure Refinement for **(BEDT-TTF)$_3$Ta$_2$F$_{10}$O, (*rac*)-(DM-EDT-TTF)$_3$Ta$_2$F$_{10}$O, (*S,S*)-(DM-EDT-TTF)$_3$Ta$_2$F$_{10}$O and (*n*-Bu$_4$N)TaF$_6$**

Compound	(BEDT-TTF)$_3$Ta$_2$F$_{10}$O	(*rac*)-(DM-EDT-TTF)$_3$Ta$_2$F$_{10}$O	(*S,S*)-(DM-EDT-TTF)$_3$Ta$_2$F$_{10}$O	(*n*-Bu$_4$N)TaF$_6$
Empirical formula	C$_{30}$H$_{24}$F$_{10}$OS$_{24}$Ta$_2$	C$_{30}$H$_{30}$F$_{10}$OS$_{18}$Ta$_2$	C$_{30}$H$_{30}$F$_{10}$OS$_{18}$Ta$_2$	C$_{16}$H$_{36}$F$_6$NTa
Molecular weight	1721.83	1535.52	1535.52	537.41
T (K)	293(2)	150.0(1)	295.0(3)	150.0(1)
Wavelength (Å)	0.71073	1.54184	1.54184	1.54184
Crystal system	Monoclinic	Monoclinic	Orthorhombic	Monoclinic
Space group	$P2_1/a$	$P2_1/c$	$P2_12_12_1$	$P2_1/c$
a (Å)	12.615(1)	12.5633(6)	10.8773(2)	9.8905(7)
b (Å)	11.984(1)	10.7252(9)	12.6267(2)	14.2131(7)
c (Å)	16.747(1)	34.292(2)	34.4236(8)	15.3276(15)
α(deg)	90	90	90	90
β(deg)	90.234(9)	93.226(5)	90	91.104(6)
γ(deg)	90	90	90	90
V (Å^3)	2531.8(3)	4613.3(5)	4727.9(2)	2154.3
Z	2	4	4	4
D_c (g cm^{-3})	2.259	2.211	2.157	1.657
F(000)	1664	2968	2968	1064
Abs coeff (mm^{-1})	5.378	16.861	16.452	9.864
Crystal size (mm^3)	0.103× 0.079 × 0.022	0.088 × 0.027 × 0.019	0.121 × 0.038 × 0.027	0.204 × 0.089 × 0.039
θ (min / max)	2.090 / 27.509	3.524 / 73.485	2.567 / 73.496	4.242 / 72.630
Transmission (min/max)	0.727 / 0.888	0.4619 / 1.000	0.5885 / 1.000	0.70558 / 1.000
Data collected/unique	27701 / 5792	18990 / 8991	29625 / 9266	5263 / 5263
Data observed	2400	4855	7849	4420
R (int)	0.1866	0.1115	0.0420	- (twin)
Flack parameter	-	-	-0.04(1)	-
GOF on F^2	0.961	1.046	1.067	1.163
Final R indices [$I > 2\sigma(I)$]	R_1 = 0.0650, wR$_2$ = 0.0740	R_1 = 0.0952, wR$_2$ = 0.2044	R1 = 0.0438, wR2 = 0.1004	R1 = 0.0539, wR2 = 0.1654
R indices (all data)	R_1 = 0.2169, wR$_2$ = 0.0942	R_1 = 0.1630, wR$_2$ = 0.2456	R1 = 0.0545, wR2 = 0.1072	R1 = 0.0617, wR2 = 0.1771
Largest peak in final: difference (e A^{-3})	1.419 / -0.958	3.059 / -2.556	1.493 / -0.733	2.440 / -3.434

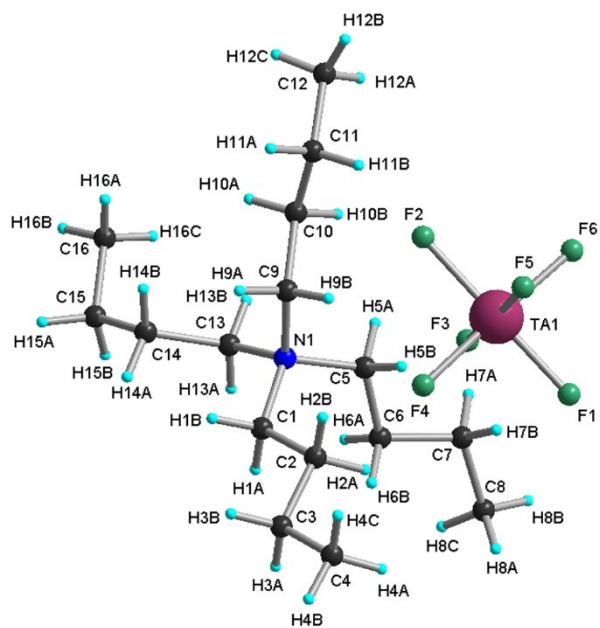## (n-Bu$_4$N)TaF$_6$

^{19}F NMR measurements
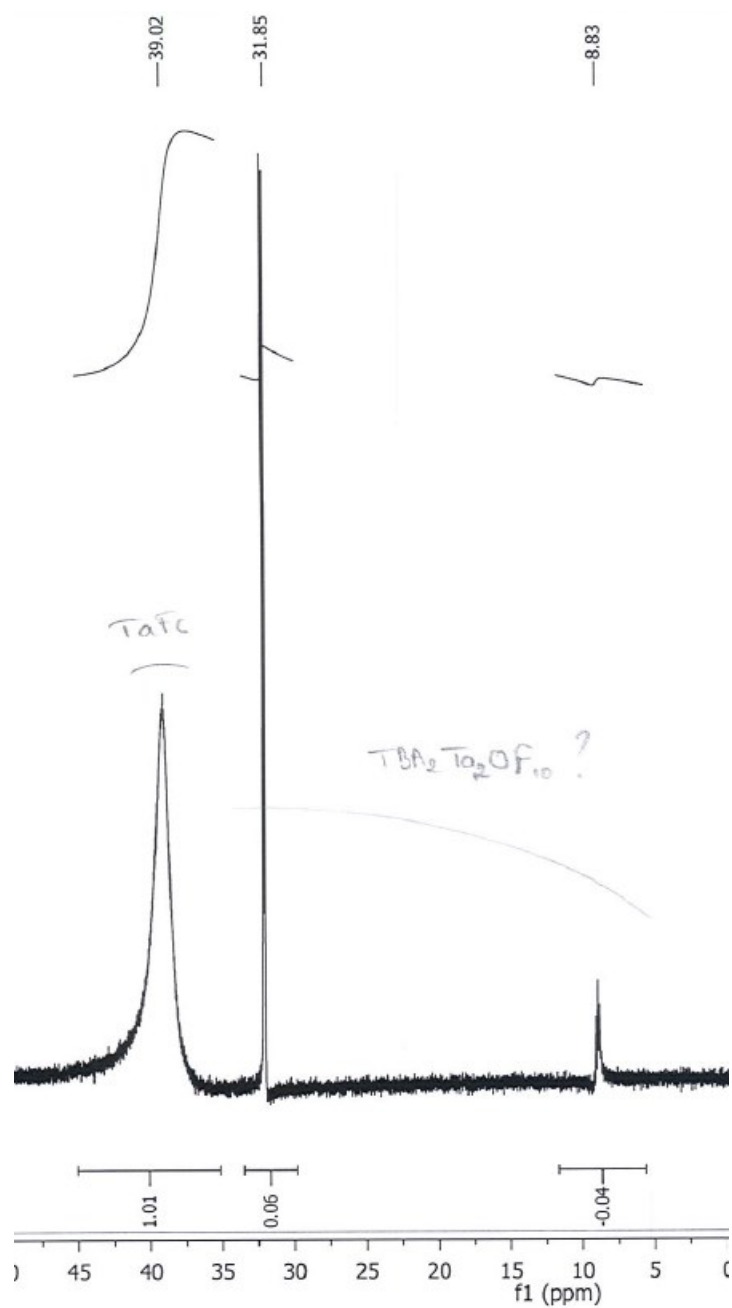
Fig. S1 ^{19}F NMR spectrum in CD$_2$Cl$_2$ of freshly prepared (n-Bu$_4$N)TaF$_6$ according to the method using metathesis of HTaF$_6$ with (n-Bu$_4$N)HSO$_4$. Ta$_2$F$_{10}$O^{2-} is already present as by-product.
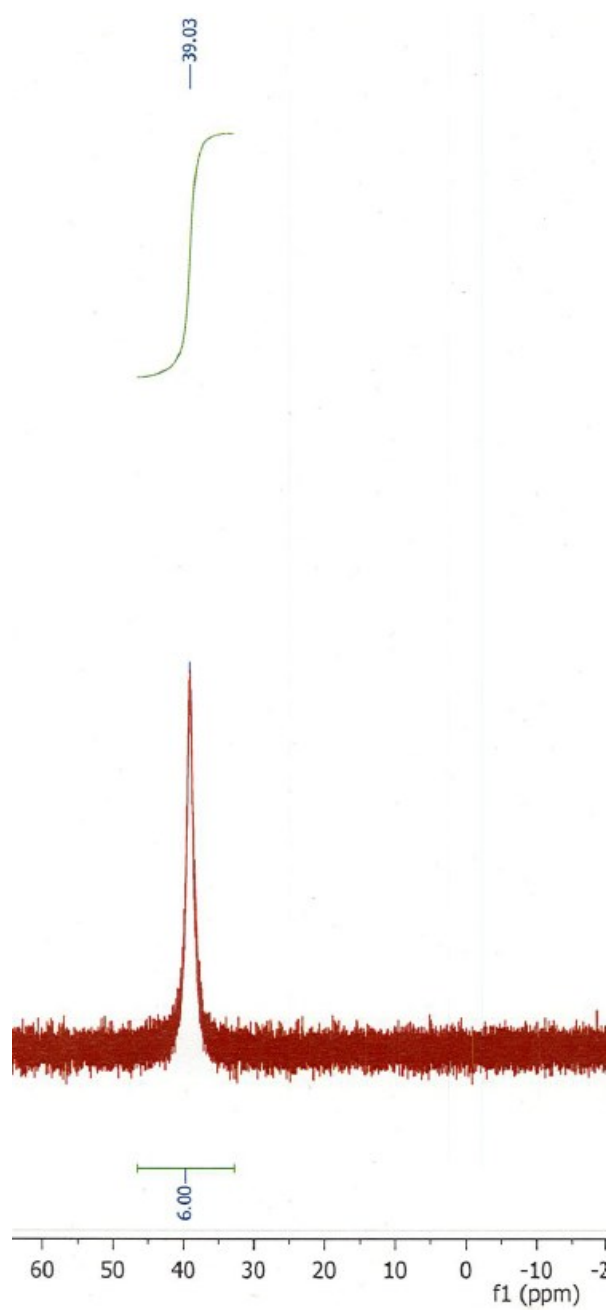
Fig. S2 ^{19}F NMR spectrum in CD_2Cl_2 of (n-Bu$_4$N)TaF$_6$ prepared according to the method using reaction of (n-Bu$_4$N)BF$_4$ with TaF$_5$.

Structural details

Fig. S3 Molecular structure of (*n*-Bu$_4$N)TaF$_6$ together with the atom numbering scheme.

(*n*-Bu₄N)₂Ta₂F₁₀O

¹⁹F NMR measurements
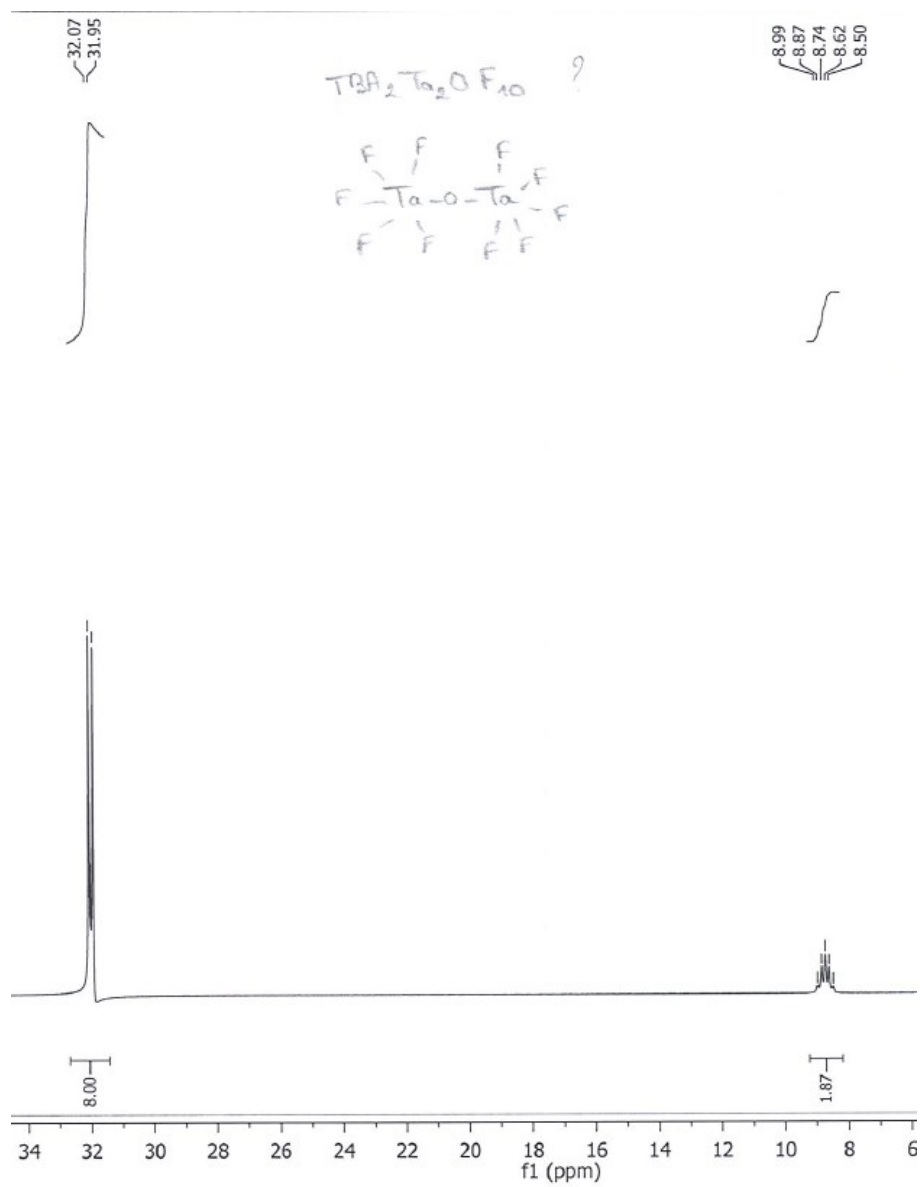
Fig. S4 ¹⁹F NMR spectrum of (*n*-Bu₄N)₂Ta₂F₁₀O in CD₂Cl₂.

Structural details
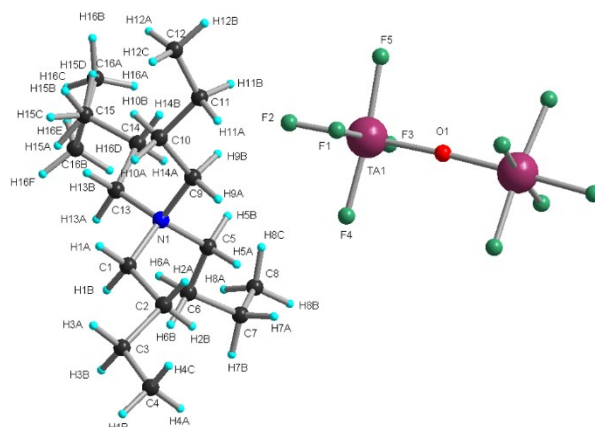
Fig. S5 Molecular structure of (n-Bu$_4$N)$_2$Ta$_2$F$_{10}$O together with the atom numbering scheme.
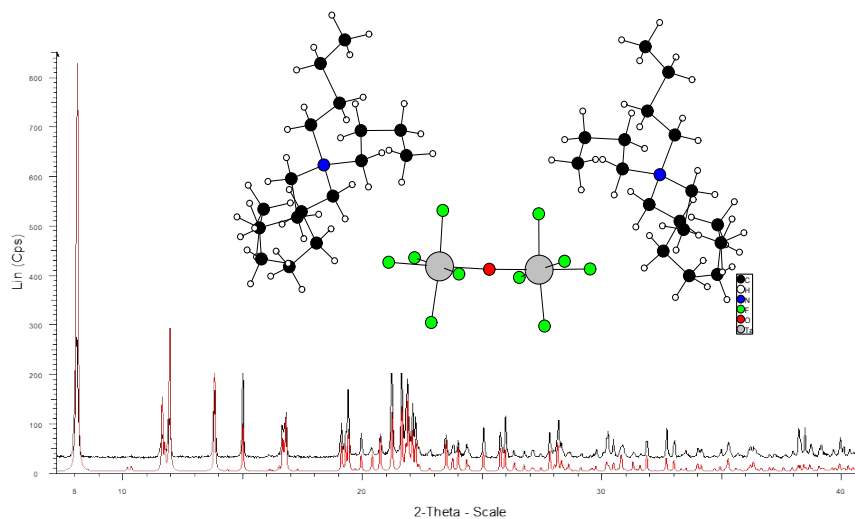
Fig. S6 X-ray powder diffractogram of (n-Bu$_4$N)$_2$Ta$_2$F$_{10}$O on polycrystalline sample (black) perfectly indexed with the simulated diffractogram from the single crystal structure (red).

Table S2 Ta–F, Ta–O distances and Ta-O-Ta angles in (n-Bu$_4$N)$_2$Ta$_2$F$_{10}$O, (TMTTF)$_3$Ta$_2$F$_{10}$O, (TMTSF)$_3$Ta$_2$F$_{10}$O and

		(n-Bu$_4$N)$_2$Ta$_2$F$_{10}$O	(TMTTF)$_3$Ta$_2$F$_{10}$O	(TMTSF)$_3$Ta$_2$F$_{10}$O	(BEDT-TTF)$_3$Ta$_2$F$_{10}$O
d (Ta—F) Å	Ta1—F1	1.893(4)	1.896(5)	1.891(3)	1.886(5)
	Ta1—F2	1.932(3)	1.900(4)	1.896(3)	1.899(4)
	Ta1—F3	1.882(4)	1.905(5)	1.901(3)	1.921(5)
	Ta1—F4	1.868(4)	1.906(5)	1.890(3)	1.877(5)
	Ta1—F5	1.887(4)	1.903(6)	1.895(3)	1.888(4)
d(Ta—O) Å	Ta1—O1	1.8884(3)	1.8923(3)	1.8905(2)	1.8976(4)
<(Ta—O—Ta) °	Ta1—O1—Ta1*	177.5(4)	180.00(1)	180	180.00(2)

(BEDT-TTF)$_3$Ta$_2$F$_{10}$O

(TMTSF)$_3$Ta$_2$F$_{10}$O and (TMTTF)$_3$Ta$_2$F$_{10}$O
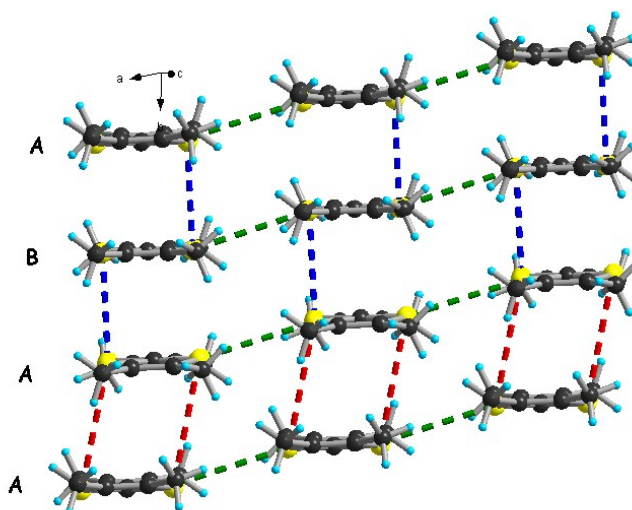
Fig. S7 Packing diagram of (TMTTF)$_3$Ta$_2$F$_{10}$O with an emphasis on the S···S short contacts: red dotted lines (4.21 Å), blue dotted lines (3.55 Å) and green dotted lines (3.86 Å).

Table S3 Selected C=C and C–S internal bond distances for (TMTSF)$_3$Ta$_2$F$_{10}$O (left) and (TMTTF)$_3$Ta$_2$F$_{10}$O (right)

Bond lengths (Å)		
(TMTSF)$_3$Ta$_2$F$_{10}$O		
A	C1—C2	1.356(6)
	Se1—C1	1.871(4)
	Se2—C1	1.887(4)
	Se3—C2	1.886(4)
	Se4—C2	1.886(4)
B	C11—C11*	1.371(8)
	Se5—C11	1.856(4)
	Se6—C11	1.877(4)

Bond lengths (Å)		
(TMTTF)$_3$Ta$_2$F$_{10}$O		
A	C1—C2	1.364(10)
	S1—C1	1.739(7)
	S2—C1	1.740(7)
	S3—C2	1.744(7)
	S4—C2	1.732(7)
B	C11—C11*	1.382(13)
	S5—C11	1.717(6)
	S6—C11	1.730(6)

(TMTSF)$_3$Ta$_2$F$_{10}$O			
Type	**C—H—F**	**d (H—F) Å**	**d(C—F) Å**	**<(C—H—F) °**
	C10—H10A—F3	2.470(3)	3.400(6)	162.98(31)
	C14—H14A—F2	2.547(3)	3.492(5)	168.07(29)
	C8—H8C—F5	2.569(4)	3.257(7)	128.74(33)
CH$_3$	C9—H9C—F3	2.698(3)	3.483(6)	139.36(32)
	C14—H14C—F1	2.723(3)	3.681(6)	175.93(30)
	C7—H7C—F5	2.752(3)	3.669(6)	160.09(33)
	C7—H7B—F1	2.813(3)	3.356(6)	116.74(34)
	C15—H15B—F4	2.868(3)	3.498(7)	124.10(31)

Table S4 C–H⋯F hydrogen bonding distances (Å) and angles in (TMTSF)$_3$Ta$_2$F$_{10}$O
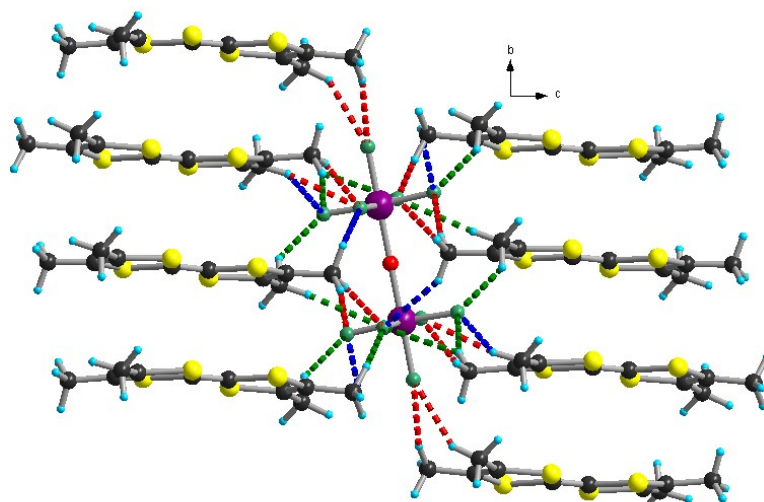
Fig. S8 CH···F short contacts in the structure of (TMTTF)$_3$Ta$_2$F$_{10}$O in the *bc* plane. Red dotted lines (2.42- 2.49-2.56 Å), blue dotted lines (2.81- 2.84- 2.86 Å) and green dotted lines (2.60- 2.65-2.67- 2.75 Å).
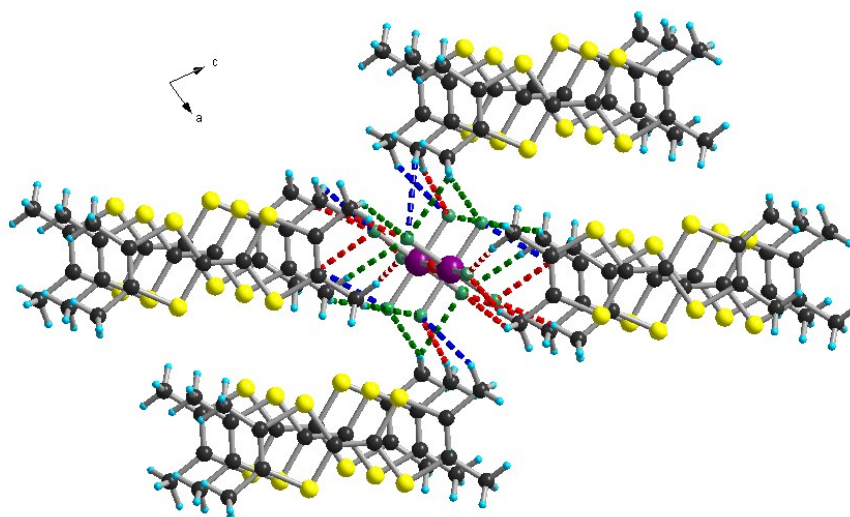
Fig. S9 CH···F short contacts in the structure of (TMTTF)$_3$Ta$_2$F$_{10}$O in the *ac* plane. Red dotted lines (2.42- 2.49-2.56 Å), blue dotted lines (2.81- 2.84- 2.86 Å) and green dotted lines (2.60- 2.65-2.67- 2.75 Å).

Table **S5** C–H⋯F

		(TMTTF)$_3$Ta$_2$F$_{10}$O		
Type	**C—H—F**	**d (H—F) Å**	**d(C—F) Å**	**<(C—H—F) °**
CH$_3$	C10—H10A—F3	2.428(5)	3.334(9)	157.25(53)
	C14—H14A—F2	2.491(5)	3.436(9)	168.04(50)
	C8—H8C—F5	2.564(7)	3.397(11)	145.19(51)
	C9—H9C—F3	2.568(5)	3.517(10)	170.12(55)
	C8—H8B—F1	2.608(7)	3.460(11)	148.09(51)
	C15—H15C—F2	2.651(5)	3.609(9)	175.91(48)
	C15—H15B—F4	2.670(7)	3.471(12)	141.20(51)
	C10—H10B—F2	2.758(5)	3.537(9)	138.75(50)
	C9—H9C—F4	2.814(5)	3.402(11)	120.42(55)
	C14—H14B—F2	2.850(5)	3.631(9)	139.24(48)
	C14—H14B—F3	2.864(6)	3.347(12)	112.21(52)

hydrogen bonding distances (Å) and angles in (TMTTF)$_3$Ta$_2$F$_{10}$O

(BEDT-TTF)$_3$Ta$_2$F$_{10}$O

Table S6 Selected C=C and C–S internal bond distances for (BEDT-TTF)$_3$Ta$_2$F$_{10}$O

Bond lengths (Å)
(BEDT-TTF)$_3$Ta$_2$F$_{10}$O

A	**C1—C2**	1.360(8)
	S1—C1	1.750(9)
	S2—C1	1.745(9)
	S3—C2	1.750(10)
	S4—C2	1.742(9)
B	**C11—C11***	1.392(13)
	S9—C11	1.727(10)
	S10—C11	1.720(10)
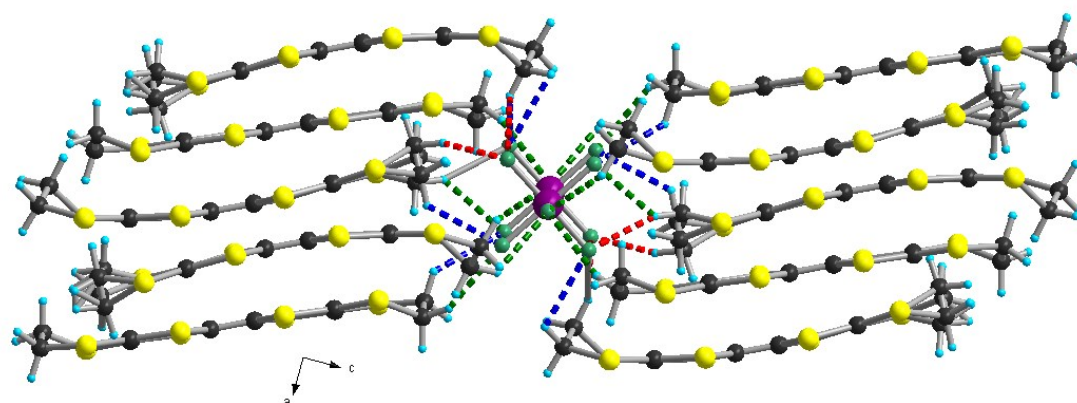
Fig. S10 CH···F short contacts in the structure of (BEDT-TTF)$_3$Ta$_2$F$_{10}$O in *ac* plane: red dotted lines (2.37- 2.56 Å), green dotted lines (2.62- 2.63-2.77 Å) and blue dotted lines (2.81- 2.85 Å).
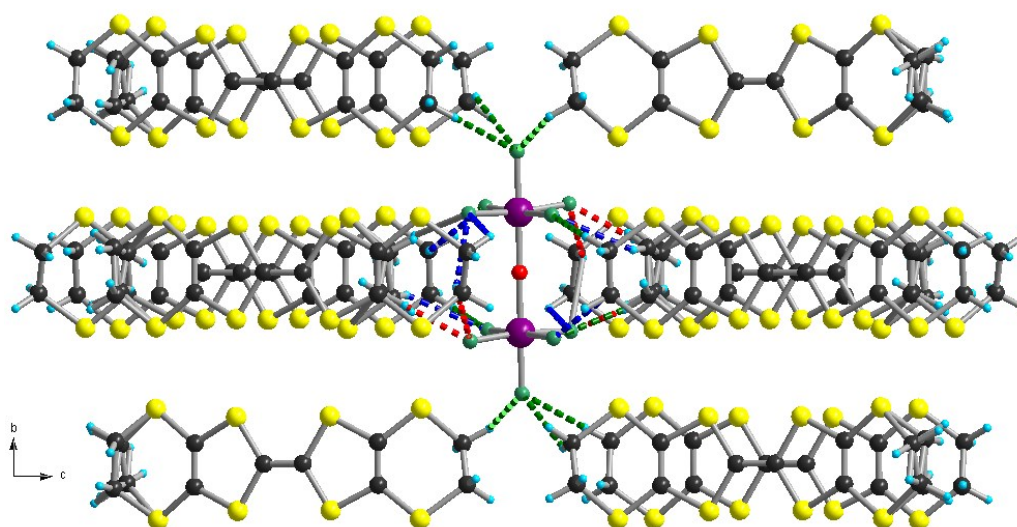

Fig. S11 CH···F short contacts in the structure of (BEDT-TTF)$_3$Ta$_2$F$_{10}$O in *bc* plane: Red dotted lines (2.37- 2.56 Å), green dotted lines (2.62- 2.63-2.77 Å) and blue dotted lines (2.81- 2.85 Å).
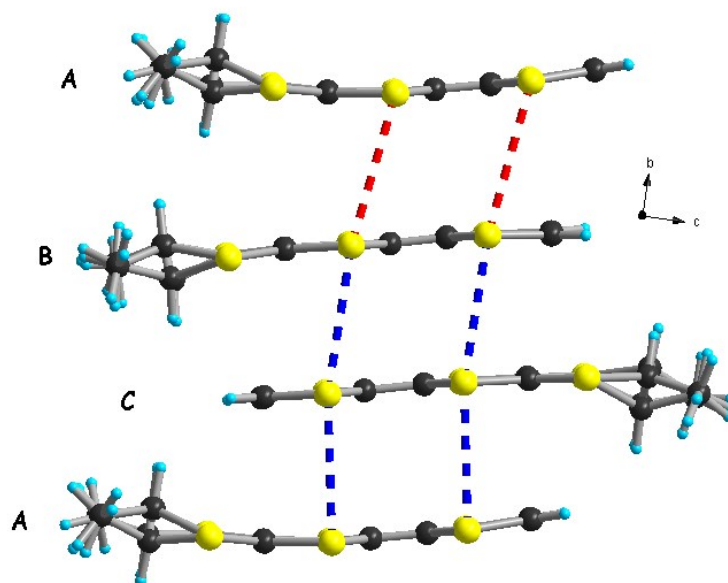
Type	C—H—F	d (H—F) Å	d(C—F) Å	<(C—H—F) °
... (BEDT-TTF)$_3$Ta$_2$F$_{10}$O				
CH$_2$	C9A—H9B—F4	2.377(6)	3.293(35)	157.2(20)
	C7—H7B—F1	2.561(6)	3.212(12)	124.53(61)
	C8—H8B—F3	2.628(6)	3.280(12)	124.85(62)
	C15—H15B—F2	2.630(5)	3.492(12)	148.07(66)
	C7—H7B—F4	2.775(8)	3.461(13)	128.36(62)
	C8—H8A—F4	2.815(5)	3.295(12)	111.46(61)
	C14—H14A—F5	2.852(6)	3.536(14)	128.22(75)

Table S7 C–H···F hydrogen bonding distances (Å) and angles in (BEDT-TTF)$_3$Ta$_2$F$_{10}$O

[(*rac*)-DM-EDT-TTF]$_3$Ta$_2$F$_{10}$O
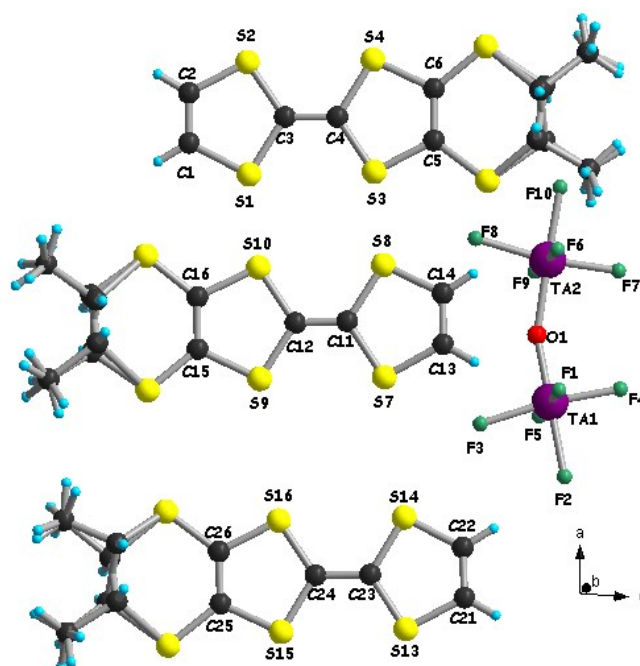
Fig. S12 Molecular structure of [(*rac*)-DM-EDT-TTF]$_3$Ta$_2$F$_{10}$O.

Table S8 Ta-F, Ta-O distances and Ta-O-Ta angles in (*n*-Bu$_4$N)$_2$Ta$_2$F$_{10}$O, [(*rac*)-DM-EDT-TTF]$_3$Ta$_2$F$_{10}$O and [(*S,S*)-DM-EDT-TTF]$_3$Ta$_2$F$_{10}$O

		(*n*-Bu$_4$N)$_2$Ta$_2$F$_{10}$O	[(*rac*)-DM-EDT-TTF]$_3$Ta$_2$F$_{10}$O	[(*S,S*)-DM-EDT-TTF]$_3$Ta$_2$F$_{10}$O
	Ta1—F1	1.893(4)	1.915(14)	1.863(8)
	Ta1—F2	1.932(3)	1.989(9)	1.890(8)
	Ta1—F3	1.882(4)	1.918(13)	1.948(5)
	Ta1—F4	1.868(4)	1.863(14)	1.925(7)
	Ta1—F5	1.887(4)	1.923(15)	1.891(8)
d (Ta—F) Å	Ta2—F6	-	1.930(13)	1.905(8)
	Ta2—F7	-	1.865(12)	1.893(8)
	Ta2—F8	-	1.955(13)	1.904(8)
	Ta2—F9	-	1.915(14)	1.916(8)
	Ta2—F10	-	1.927(10)	1.911(9)
d(Ta—O) Å	Ta1—O1	1.8884(3)	1.788(13)	1.863(9)
	Ta2—O1	-	1.974(11)	1.916(9)
<(Ta—O—Ta) °	Ta1—O1—Ta2	177.5(4)	161.1(8)	156.7(6)

Fig. S13 Packing diagram of [(*rac*)-DM-EDT-TTF]$_3$Ta$_2$F$_{10}$O with an emphasis on the S···S short contacts along *b*: red dotted lines (3.74 – 3.75 Å) and blue dotted lines (3.48 – 3.52 Å).
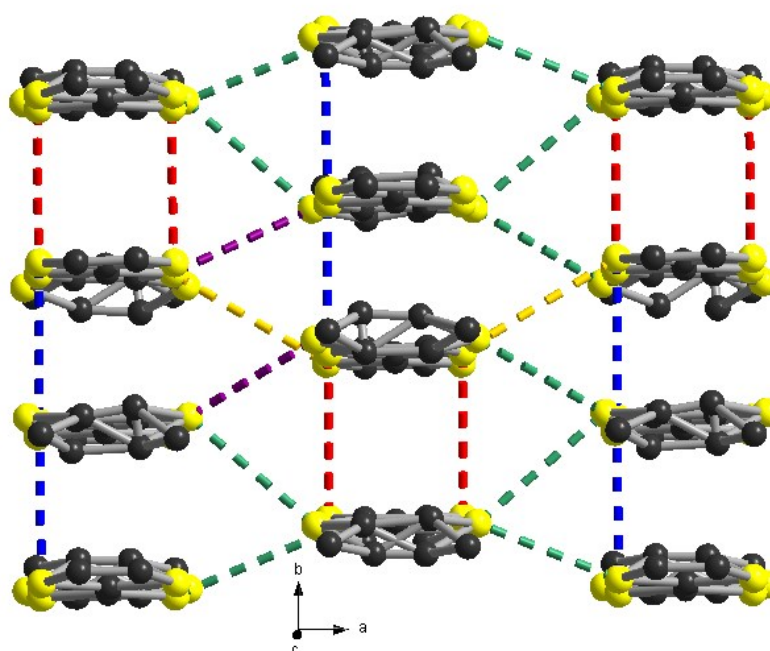
Fig. S14 Packing diagram of [(*rac*)-DM-EDT-TTF]$_3$Ta$_2$F$_{10}$O with an emphasis on the S···S short contacts in the *ab* plane: red dotted lines (3.74 – 3.75 Å), blue dotted lines (3.48 – 3.52 Å), green dotted lines (3.61 – 3.63 – 3.67 – 3.70 Å), violet dotted lines (3.58 – 3.59 Å) and yellow dotted lines (4.05 Å). Hydrogen atoms are omitted for clarity.
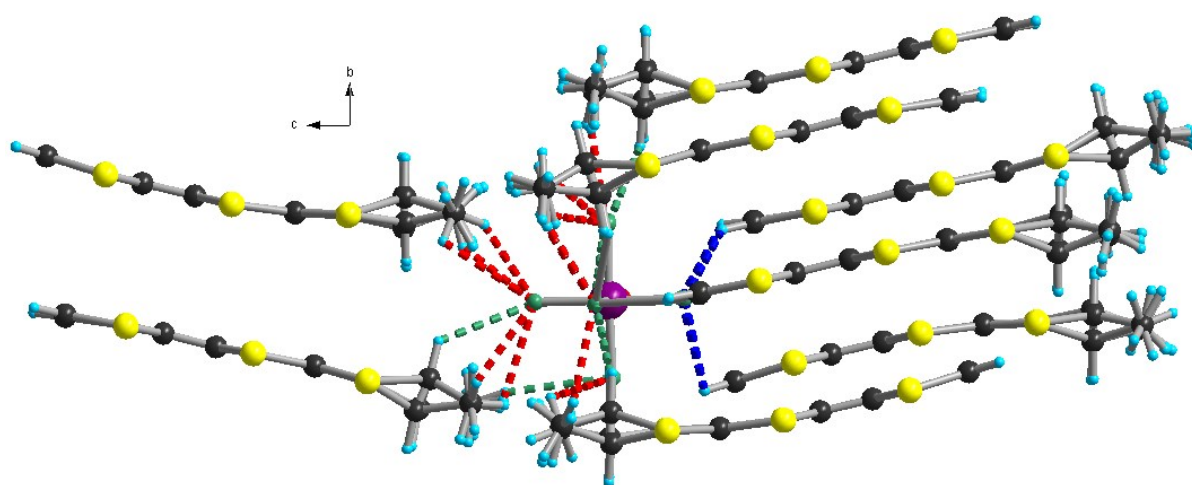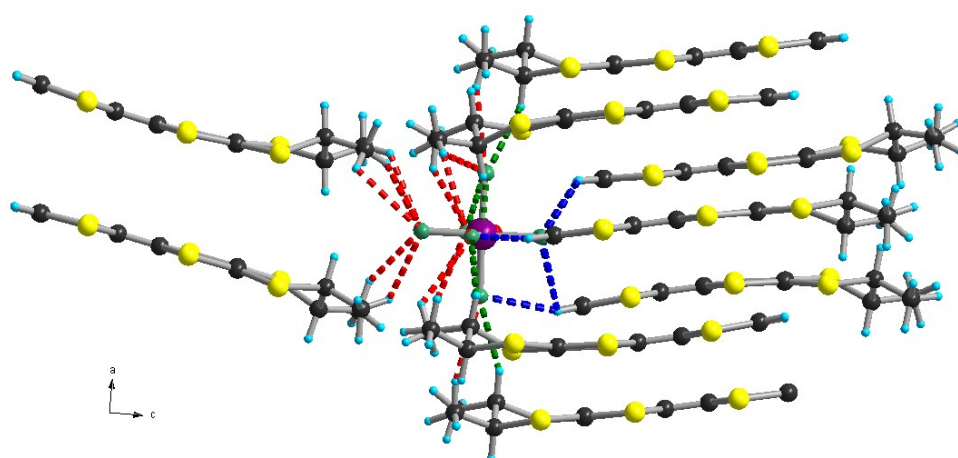
Fig. S15 Solid state structure of [(*rac*)-DM-EDT-TTF]$_3$Ta$_2$F$_{10}$O with an emphasis on the C–H⋯F short contacts: blue dotted lines for CH vinyl (2.36- 2.42- 2.67 Å), red dotted lines for Me (2.42- 2.51- 2.61- 2.71- 2.78 Å) and green dotted lines for H$_{CH}$ (2.72- 2.73 Å), in the *bc* plane.

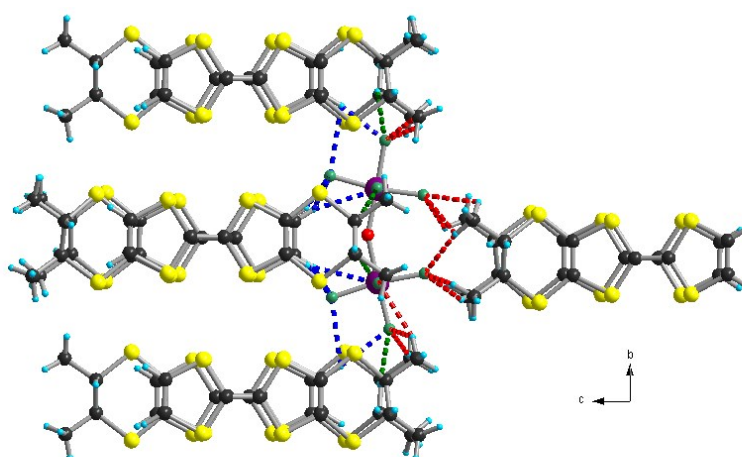| [(*rac*)-DM-EDT-TTF]$_3$Ta$_2$F$_{10}$O				
Type	**C—H—F**	**d (H—F) Å**	**d(C—F) Å**	**<(C—H—F) °**
CH $_{vinyl}$	C1—H1—F8	2.366(13)	3.129(26)	139.3(14)
	C2—H2—F3	2.423(14)	3.141(25)	133.9(13)
	C21—H21—F10	2.244(10)	3.161(23)	168.8(13)
	C13—H13—F3	2.677(14)	3.002(33)	101.2(18)
CH$_3$	C30—H30D—F5	2.428(15)	3.314(35)	153.0(19)
	C9—H9A—F7	2.516(15)	3.205(26)	129.0(13)
	C10—H10A—F4	2.610(14)	3.168(26)	117.3(13)
	C20—H20D—F7	2.787(14)	3.207(33)	107.3(17)
	C20—H20F—F4	2.712(13)	3.579(31)	149.7(17)
CH	C17A—H17A—F2	2.722(11)	3.341(43)	121.8(24)
	C7A—H7A—F4	2.730(13)	3.420(39)	127.7(22)

Table S9 C–H⋯F hydrogen bonding distances (Å) and angles in [(*rac*)-DM-EDT-TTF]$_3$Ta$_2$F$_{10}$O

[(*S*,*S*)-DM-EDT-TTF]$_3$Ta$_2$F$_{10}$O

Fig. S16 Solid state structure of [(*S*,*S*)-DM-EDT-TTF]$_3$Ta$_2$F$_{10}$O, with an emphasis on the C–H···F short contacts: blue dotted lines for CH vinyl (2.22- 2.40- 2.44- 2.53 Å), red dotted lines for Me (2.46- 2.58- 2.65- 2.82 Å) and green dotted lines for H$_{CH}$ (2.66- 2.75 Å), in the *ac* plane.

Fig. S17 Solid state structure of [(*S*,*S*)-DM-EDT-TTF]$_3$Ta$_2$F$_{10}$O, with an emphasis on the C–H···F short contacts: blue dotted lines for CH vinyl (2.22- 2.40- 2.44- 2.53 Å), red dotted lines for Me (2.46- 2.58- 2.65- 2.82 Å) and green dotted lines for H$_{CH}$ (2.66- 2.75 Å), in the *ac* plane.

[(*S,S*)-DM-EDT-TTF]$_3$Ta$_2$F$_{10}$O				
Type	C—H—F	d (H—F) Å	d(C—F) Å	<(C—H—F) °
CH $_{vinyl}$	C1B—H1B—F8	2.222(6)	3.139(14)	169.1(8)
	F9—H2C—C2C	2.442(11)	3.165(21)	134.4(11)
	F4—H1C—C1C	2.401(10)	3.144(20)	136.6(11)
	F7—H2A—C2A	2.531(13)	3.396(25)	155.1(13)
CH$_3$	F2—H10A—C10C	2.466(10)	3.250(23)	139.2(12)
	F2—H10I—C10A	2.582(11)	3.253(22)	127.2(12)
	F3—H9B1—C9B	2.654(8)	3.535(22)	152.8(12)
	F6—H9C3—C9C	2.674(13)	3.196(20)	114.6(10)
	F6—H9A1—C9A	2.822(10)	3.241(22)	107.4(11)
CH	F8—H7A—C7A	2.668(7)	3.313(15)	123.6(8)
	F10—H8B—C8B	2.757(9)	3.478(17)	130.8(9)

**Table S10** C–H···F hydrogen bonding distances (Å) and angles in [(*S,S*)-DM-EDT-TTF]$_3$Ta$_2$F$_{10}$O

Table S11 Selected C=C and C–S internal bond distances for [(*S,S*)-DM-EDT-TTF]$_3$Ta$_2$F$_{10}$O and [(*rac*)-DM-EDT-

Bond lengths (Å)					
[(*S,S*)- DM-EDT-TTF]$_3$Ta$_2$OF$_{10}$			[(*rac*)- DM-EDT-TTF]$_3$Ta$_2$OF$_{10}$		
A	C3A—C4A	1.370(19)	A	C3—C4	1.35(3)
	S1A—C3A	1.724(16)		S1—C3	1.766(18)
	S2A—C3A	1.723(16)		S2—C3	1.732(18)
	S3A—C4A	1.741(14)		S3—C4	1.722(19)
	S4A—C4A	1.723(15)		S4—C4	1.76(2)
B	C3B—C4B	1.368(16)	B	C11—C12	1.34(4)
	S1B—C3B	1.737(12)		S7—C11	1.75(2)
	S2B—C3B	1.725(12)		S8—C11	1.73(2)
	S3B—C4B	1.732(12)		S9—C12	1.73(3)
	S4B—C4B	1.728(12)		S10—C12	1.74(2)
C	C3C—C4C	1.350(17)	C	C23—C24	1.41(3)
	S1C—C3C	1.743(13)		S13—C23	1.70(18)
	S2C—C3C	1.739(14)		S14—C23	1.73(2)
	S3C—C4C	1.743(12)		S15—C24	1.721(19)
	S4C—C4C	1.733(13)		S16—C24	1.72(2)

TTF]$_3$Ta$_2$F$_{10}$O.

**Conductivity measurements**

Electrical resistivity was measured in four points on platelet-shaped single crystals 0.5-0.8 mm long for $(TMTSF)_3Ta_2OF_{10}$, $(TMTTF)_3Ta_2OF_{10}$ and (rac)-$(DM$-EDT-$TTF)_3Ta_2OF_{10}$. Gold wires were glued with silver paste on aligned gold evaporated contacts. For the platelets of $(BEDT$-$TTF)_3Ta_2OF_{10}$ (0.3-0.4 mm long), it was not possible to evaporate gold contacts on so small samples. Therefore, the four electrical contacts used to measure the in-plane resistivity were point contacts made by silver paste. Because of the small size of the (rac)-$(DM$-EDT-$TTF)_3Ta_2F_{10}O$ crystals (maximum length of 0.25 mm), their resistance was measured in two points with gold wires directly attached on both ends of the crystals. Different techniques were used to measure resistivity, either applying a low frequency ($\approx$ 100 Hz) AC current (1 - 10 µA) with lock-in amplifier detection or a DC current (1 - 0.1 µA). We have checked for each crystal that both techniques give the same resistance value at room temperature. Low temperature was provided either by a homemade cryostat equipped with a 4 K pulse-tube or using a Quantum Design Physical Property Measurement System (PPMS).
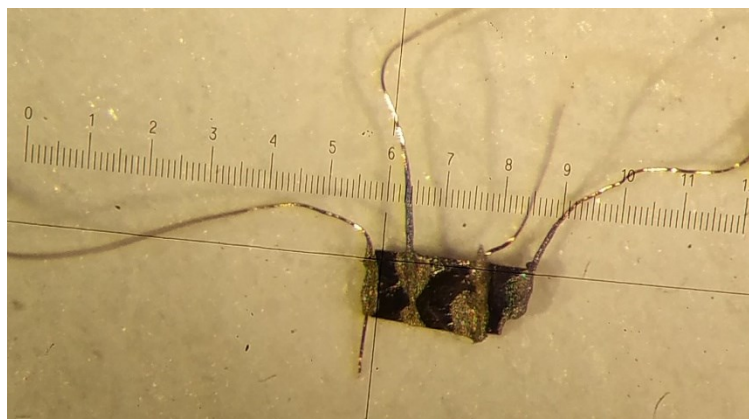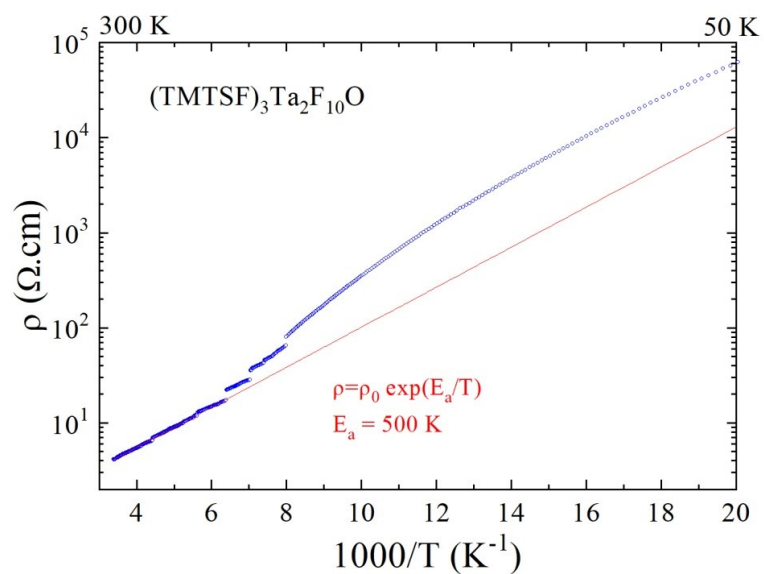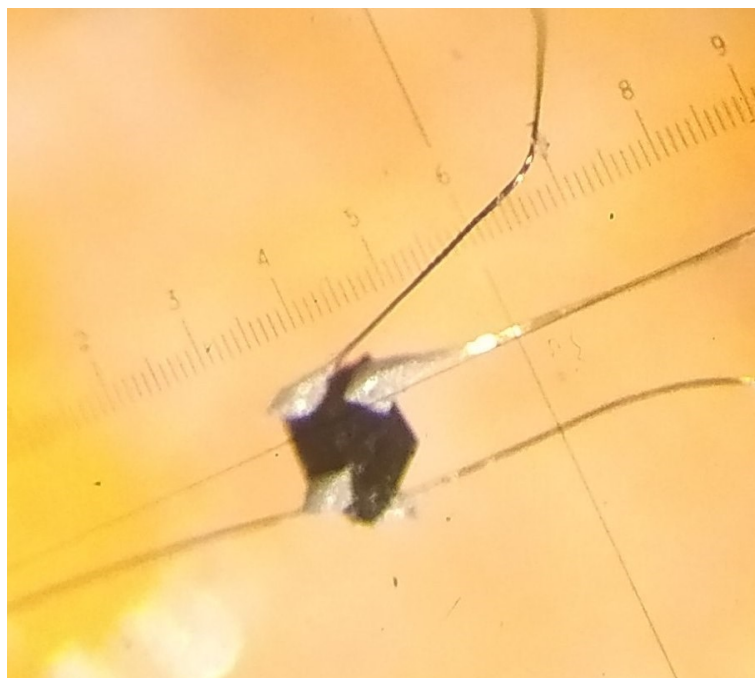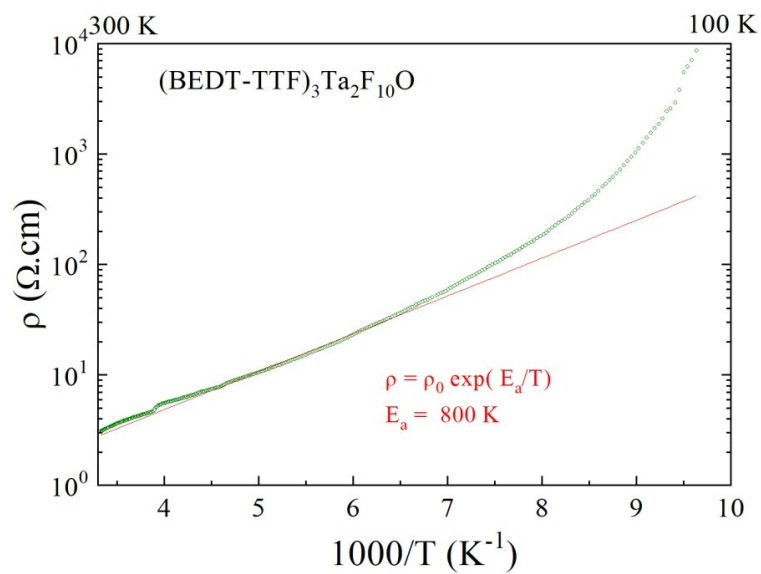
Fig. S18 Temperature dependence of the electrical resistivity plotted as log ρ *versus* 1/T for a single crystal of (TMTSF)$_3$Ta$_2$F$_{10}$O (top). The red line is the linear fit giving the activation energy from the law ρ = ρ$_0$ exp(E$_a$/T) determined in the temperature range 160 – 300 K. The small jumps on the resistivity curve are due to microcracks in the crystal occurring during cooling down. Picture of the crystal with the four aligned gold contacts (bottom).
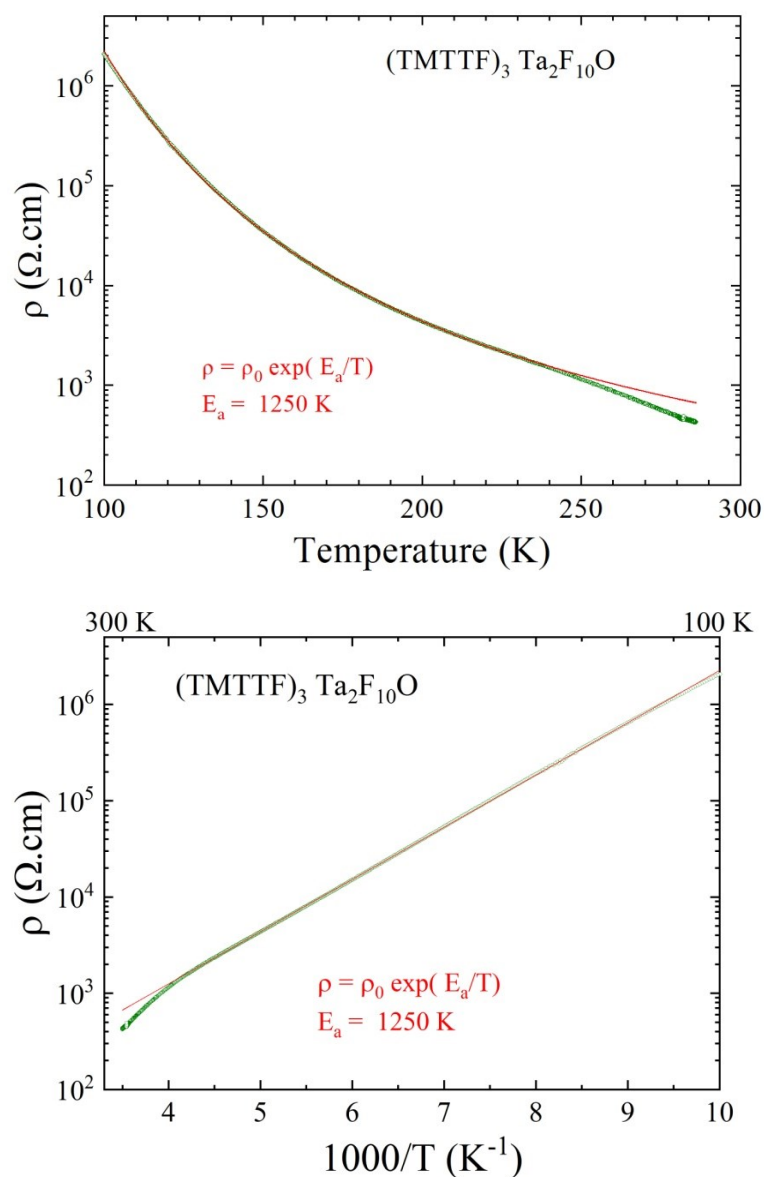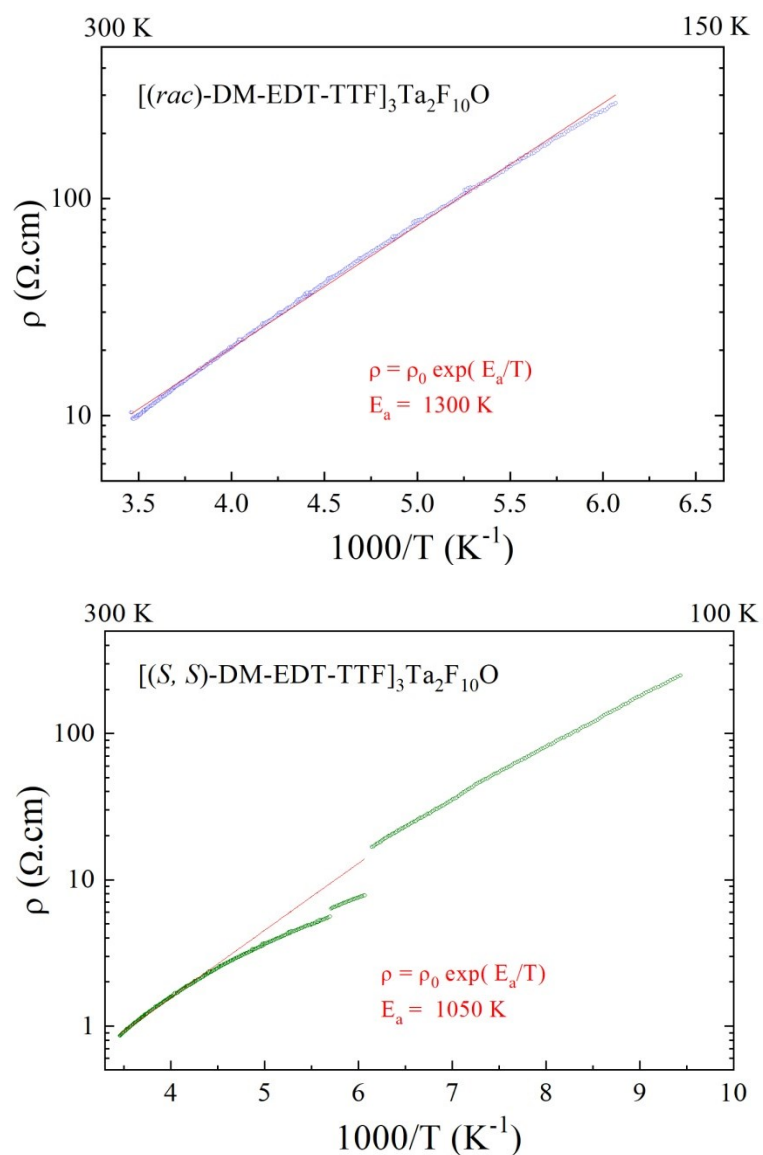
Fig. S19 Temperature dependence of the electrical resistivity plotted as log ρ *versus* T (top) and as log ρ *versus* 1/T (bottom) for a single crystal of $(TMTTF)_3Ta_2F_{10}O$. The red line is the linear fit giving the activation energy from the law $\rho = \rho_0 \exp(E_a/T)$ determined in the temperature range $100 - 290$ K.

Fig. S20 Temperature dependence of the electrical resistivity plotted as log ρ *versus* 1/T for a single crystal of (BEDT-TTF)$_3$Ta$_2$F$_{10}$O (top). The red line is the linear fit giving the activation energy from the law $\rho = \rho_0 \exp(E_a/T)$ determined in the temperature range 135 – 300 K. Picture of the crystal used to measure the in-plane resistivity with the four contacts (bottom).

Fig. S21 Temperature dependence of the electrical resistivity plotted as log ρ *versus* 1/T for a single crystal of [(*rac*)-DM-EDT-TTF]$_3$Ta$_2$F$_{10}$O (top) and for a single crystal of [(*S*,*S*)-DM-EDT-TTF]$_3$Ta$_2$F$_{10}$O (bottom). The red line is the linear fit giving the activation energy from the law ρ = ρ$_0$ exp(E$_a$/T)) determined in the temperature range 165 – 290 K (top) and 200 – 290 K (bottom). The small jumps on the resistivity curve of (*S*,*S*) enantiopure salt are due to microcracks in the crystal occurring during the cooling down.

Band structure calculations
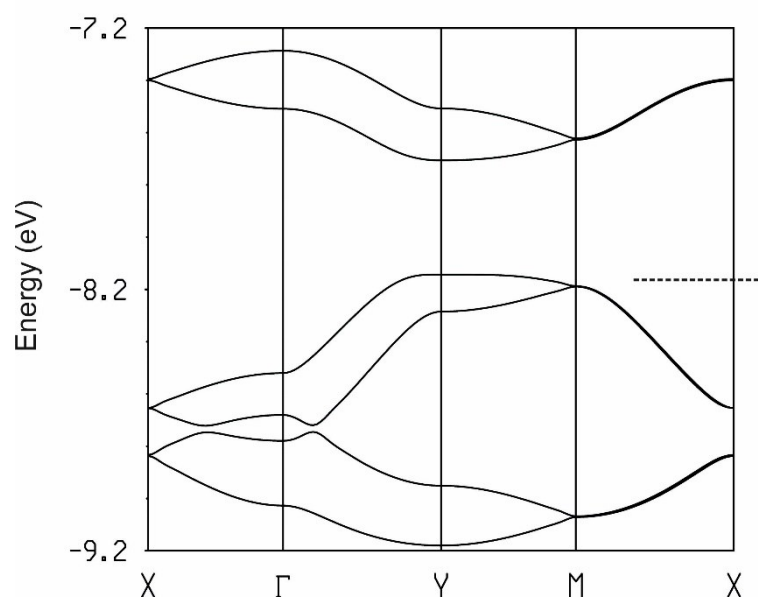
Fig. S22 Calculated band structure for the donor layers of (*rac*)-(DM-EDT-TTF)$_3$Ta$_2$F$_{10}$O where the dashed line refers to the highest occupied level and Γ = (0, 0), X = (a^*/2, 0), Y = (0, b^*/2), M = (a^*/2, b^*/2) and S = (-a^*/2, b^*/2). Note that the *a* and *b* axes have been interchanged with respect to those used for the (*S*,*S*) enantiomer salt (Fig. 15).